International Journal of Environmental Science and Technology (2022) 19:727–746
https://doi.org/10.1007/s13762-021-03582-x

ORIGINAL PAPER

NiO and MgO/activated carbon as an efficient CO_2 adsorbent: characterization, modeling, and optimization

A. Ghaemi[1] · H. Mashhadimoslem[1] · P. Zohourian Izadpanah[1]

Received: 21 July 2020 / Revised: 28 June 2021 / Accepted: 25 July 2021 / Published online: 11 August 2021

Abstract

In this research, activated carbon (AC)-based absorbents modified with NiO and MgO were prepared by wet impregnation method for adsorption of carbon dioxide (CO_2). The effect of adding ($Ni(NO_3)_2$ $6(H_2O)$) and ($Mg(NO_3)_2$ $6(H_2O)$) in 1, 3, 5, and 7 wt% to AC was studied. Raw AC and modified AC were characterized by ultimate analysis, scanning electron microscopy, X-ray diffraction, and surface area. In addition, response surface methodology method was used to optimize the adsorption operation condition. The five-level central composite design was applied to design the experiments for three types of adsorbents (AC, AC/NiO-3, and AC/MgO-3) in the temperature and pressure ranges of 25–80 °C and 2–10 bar, respectively. The results indicated that the adsorption capacity of activated carbon was modified after NiO and MgO loading, especially at higher temperatures, and the optimal concentrations were obtained 3 wt% for both of them. For better evaluation of the adsorbents behavior, experimental data were investigated by isotherm, kinetic, and thermodynamic models. The optimum adsorption capacities were obtained 121.35, 105.17 mg/g for AC/NiO-3 and AC/MgO-3, respectively.

Keywords CO_2 · Adsorption · Activated carbon · Metal oxides · Optimization

Introduction

The emission of greenhouse gases is one of the major environmental problems in recent decades that would increase by about 30% by 2040 (Míguez et al. 2018). Carbon dioxide (CO_2) as the most significant greenhouse gas, which has been released into the atmosphere from the burning of fossil fuels, has the largest share in the global warming. Therefore, CO_2 capture technologies can be very helpful to reduce CO_2 emissions from flue gas and prevent an increase in the earth's temperature (Taheri et al. 2019; Wang et al. 2011).

Adsorption (Khajeh and Ghaemi 2019; Mohammad et al. 2019), absorption (Heydarifard et al. 2018; Norouzbahari et al. 2016), membrane diffusion (Shekhawat et al. 2003), and cryogenics (Tuinier et al. 2010) are considered as the main methods for CO_2 capture and separation (Bahadori and Vuthaluru 2009). The capture of CO_2 by adsorption method is of great interest due to the low cost of equipment, low energy consumption, and simplicity of application (Fenrong, et al. 2010). Choosing the right adsorbent for adsorption is of great importance. Activated carbon (AC) is a very effective and suitable material among the many solid adsorbents and extensively used for CO_2 adsorption because of its low cost, large activated surface area, developed porous structure, low sensitivity, and high thermal stability (Herawan et al. 2013; Karbalaei Mohammad et al. 2019; Siriwardane, et al. 2001). AC is often used to adsorb CO_2 at ambient temperature, and there is a weak interaction based on physisorption process (Siriwardane et al. 2001; Younas et al. 2016). Therefore, a number of researches have been devoted to modify the AC surface by loading of metal oxides and improve interaction based on chemisorption (Hakim et al. 2015; Rashidi and Yusup 2016). Transition metals (i.e., Cu, Co, Ni, Fe, Cr) (Fenrong et al. 2010; Hakim et al. 2015; Hosseini et al. 2015; Jang and Park 2012a, b; Kim et al. 2010) and alkaline earth metals (i.e., Mg, Ca) (Pietrzak and Morawski 2013; Son et al. 2005; Yong et al. 2001) have been used to modify porous carbons, especially AC.

CO_2 is a Lewis acid in that it accepts electron from electron donors (Versteeg and Van Swaaij 1988). Since metal

Editorial responsibility Samareh Mirkia.

✉ A. Ghaemi
aghaemi@iust.ac.ir

[1] School of Chemical, Petroleum and Gas Engineering, Iran University of Science and Technology, P.O. Box 16765-163, Tehran, Iran

oxides are classified as electron donors, they may be a good option to improve the adsorption capacity of AC (Rashidi and Yusup 2016). The deposition of metal oxides in the pores of the AC surface causes a chemical reaction between the metal oxide and the CO_2 molecules. Although surface area and pore volume of adsorbent are important, they are not the only effective parameters on the adsorption capability. Studies have reported that metal oxide loading on AC reduces BET surface area and pore volume but increases the adsorption capacity because the reaction between CO_2 and adsorbate is another key factor. It seems that using an appropriate amount of metal is one of the factors that should be considered in impregnated AC. Low loading of metal on AC limits the change of surface, while the higher addition blocks microporous adsorbents and abates the adsorption capacity (Fenrong et al. 2010). In most reports, the wet impregnated method (Deraz 2018) has been used to disperse metals to the surface of activated carbon (Adamski et al. 2007; Henning and Schäfer 1993; Madzaki et al. 2018). Among the various metal salts, including nitrates, chlorides, acetates, and acetylacetonates, nitrates are highly soluble and may be more efficacious (Schwickardi et al. 2002). So far, many studies have been done on the adsorption of AC, but according to studies, AC is suitable for adsorption at ambient temperature. Therefore, two methods of nitrogen doping (Houshmand et al. 2011; Shafeeyan et al. 2011; Shafeeyan et al. 2012; Hidayu and Muda 2016) and metal impregnation have been used to improve CO2 the adsorption capacity from flue gas. Based on previous research, most articles have been presented on the study of adsorbent charactrizations. No information is provided on the study of adsorbent behavior in terms of isotherms, kinetics, and thermodynamics. Therefore, in this study, the use of modified AC with different percentages of NiO and MgO at different pressures and temperatures is considered to find an optimal operating temperature and pressure of the adsorption process. The adsorbents behavior was analyzed using isotherm, kinetic, and thermodynamic models. response surface methodology (RSM)-based central composite design (CCD) was applied to study the optimal values of parameters, the impact of operating conditions, and their interactions on response and achieving optimal conditions. This work has presented a robust and efficient hybrid approach to experimental and simulation of a transition metal and an alkaline earth metal as a modifier for CO_2 capture efficiency by AC impregnated.

Materials and methods

Materials

Commercial granule coal activated carbon (AC) with 12–40 mesh size was purchased from Mahab zist company (Tehran, Iran). High purity commercial powder nickel nitrate hexahydrate ($Ni(NO_3)_2$ $6(H_2O)$) and magnesium nitrate hexahydrate ($Mg(NO_3)_2.6(H_2O)$) were used as the metal oxide precursors. The high purity carbon dioxide (> 99.9%) was purchased from Hamta gas Mehrabad company (Tehran, Iran).

Adsorbent modification

The adsorbent is prepared by the wet impregnation method. Initially, the ACs were washed with distilled water and dried in a vacuum oven at 85 °C for 6 h. The amount of 100 ml of 1, 3, 5, and 7 wt% magnesium nitrate hexahydrate and nickel nitrate hexahydrate solution with 5 gr of dried AC was stirred for 2 h at 70 °C. The mixture was evaporated at room temperature and then dried at 85 °C for 6 h. The AC samples impregnated with nickel nitrate hexahydrate and magnesium nitrate hexahydrate are calcined under N_2 atmosphere for 2 h at 350 °C (Brockner, et al. 2007; Mikuli, et al. 2001) and 500 °C (Gardner and Messing 1984) for 2 h, respectively, to decompose the nitrate. Finally, the absorbents are stored in a desiccator.

Adsorbent characterization

The samples are characterized by various conventional techniques. An X-ray diffraction analysis (XRD) by STOE STADI-MP Germany model with Cu-Kα radiation, the voltage of 40 kV, and emission of 30 mA at room temperature is used to investigate the formation of metal oxide on the surface of AC. The surface morphology of adsorbent is studied by VEGA\TESCAN scanning electron microscopy (SEM). Also, N_2 adsorption and desorption analysis by an automatic gas adsorption system (Micromeritics, Model ASAP 2020, USA) is applied to analyze the specific surface area, distribution of pore size, total pore area, and total pore volume of mesoporous materials.

CO_2 adsorption procedure

A stainless steel reactor, as shown in Fig. 1, is used to investigate the CO_2 adsorption capacity and the influence of main parameters on the adsorption process. The cylindrical bed reactor has 160 cm^3 internal volume, and there is a cell inside the reactor to hold 1 gr of the absorbent in each test. Before performing the test, the adsorbent is preheated under pure N_2 gas for 30 min at 110 °C and vacuumed for 40 min to make sure there is no pre-adsorbed CO_2 and moisture. A high purity CO_2 gas goes through the regulator and pressure gauge to reach the required pressure and then enters the mixing tank. The gas is injected from the mixing tank into the reactor that had been quenched to ambient temperature, and then, the inlet valve is closed. An electric heater supplies the heat required for the reactor, and a thermostat regulates

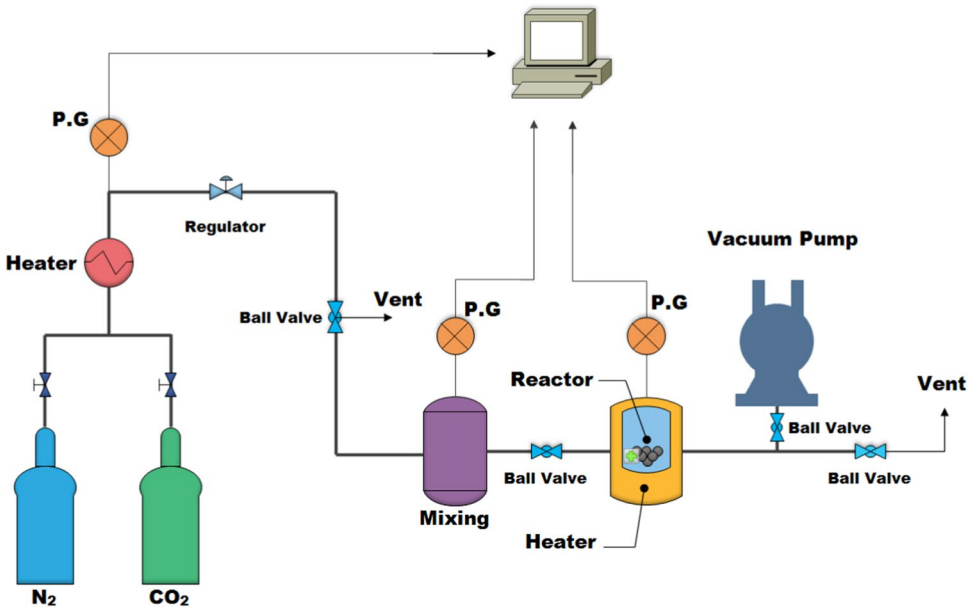

Fig. 1 Setup for CO_2 adsorption measurement

the temperature. Each run is taken one hour, and a computer records the temperature, pressure, and time every second in Excel tables.

Equation (1) can be used to calculate the adsorption capacity of the adsorbent:

$$q_e = \frac{(P_i - P_f)VM_{CO_2}}{RTZm} \times 1000 \tag{1}$$

where P_i, P_f, V, M_{CO2}, R, T, Z, and m are initial pressure, equilibrium pressure, reactor volume, the molecular weight of CO_2, gas constant, temperature, compressibility factor, and adsorbent weight, respectively. The truncated virial equation, which includes two terms, is used to calculate the compressibility factor. The second virial coefficient theoretically illustrates the Tsonopoulos equation and considers the contribution of the pair-wise potential to the gas pressure. The correlation coefficient (R^2), which represents the percentage of change in the dependent variable, is one of the reliable parameters to analyze the validity of experimental adsorption data. It can be used to determine the fitting degree of kinetic and isotherm models with laboratory data (see Eq. (2)) (Saeidi, et al. 2018).

$$R^2 = \frac{\sum \left(q_{e,\mathrm{cal}} - q_{m,\mathrm{exp}}\right)^2}{\sum \left(q_{e,\mathrm{cal}} - q_{m,\mathrm{exp}}\right)^2 + \left(q_{\mathrm{cal}} - q_{m,\mathrm{exp}}\right)^2} \tag{2}$$

where $q_{e,\mathrm{cal}}$ (mg/g), q_{exp} (mg/g), and $q_{m,\mathrm{exp}}$ (mg/g) are the adsorption capacity obtained by kinetic isotherm models, the adsorption capacity during the experiment and the average of q_{exp}, respectively.

Experimental design

The experimental design of the CO_2 adsorption process is performed using RSM method, which is a combination of statistical and mathematical techniques for analyzing the experimental data and process optimization (Pashaei et al. 2020). RSM method selects the minimum number of tests and the best conditions among many input variables that affect process performance (Sarrai et al. 2016). Central composite design (CCD) is the best-known class of RSM that has been frequently used as an experimental design (Amiri et al. 2017; Saeidi et al. 2019). According to Table 1, experiment conditions and the domain and levels of pressure (A) and temperature (B) variables are investigated at five levels with

Table 1 Optimization of parameters, experimental range, and level of independent variables

Factors	Name	Units	Symbol	Coded level				
				−2	−1	0	+1	+2
Pressure	P	bar	A	1	2.2	5	7.8	9
Temperature	T	°C	B	25	33	52.5	72	80
Absorbent			C	Absorbent type				
				AC		AC/NiO-3		AC/MgO-3

codes − 2, − 1, 0, + 1, and + 2 for three types of absorbent (C). Based on CCD, 39 runs have been designed.

For description of the experimental results by a quadratic polynomial regression model, the following second-order equation obtained from the CCD model is proposed:

$$y = a_0 + \sum_{i=1}^{n} a_i x_i + \sum_{i=1}^{n} a_{ii} x_i^2 + \sum_{i}^{n} \sum_{j}^{n} a_{ij} x_i x_{j_{i<j}} + \varepsilon \quad (3)$$

where y, i and j, x_i and x_j, a_i and a_j, a_{ij}, a_0, n, and ε represent the predicted response, index numbers for factors, design variables, coefficients of first-order effect, coefficient of interaction, constant coefficient, number of factors, and unanticipated error, respectively (Amiri et al. 2017).

Results and discussion

Adsorbent characterization

SEM image of samples at two scales, including 10 and 20 µm, is shown in Fig. 2. Based on Fig. 2a–b, the structure of raw AC is very porous and consists of different pore sizes. The morphology of AC/NiO-3 and AC/MgO-3 samples is also illustrated in Fig. 2c–f, respectively. It is evident that nickel oxide and magnesium oxide have been distributed irregularly on the surface of AC. The smaller pore size of AC is also due to the blockage of nickel oxide and magnesium oxide.

The XRD patterns of raw AC and AC impregnated with 3, 5, and 7 wt% of selected metal oxides are presented in Fig. 3a–b. The AC exhibits two different broad peaks of the graphitic structure at 2Θ = 24° and 44°, which are assigned to (002) and (100) planes. It can be seen that the intensity of these peaks gets weaker, and the noise level increases with increase in the metal oxide loading. There is no peak related to metal oxides in the AC/NiO-3 and AC/MgO-3 samples, due to the lack of sensitivity of this technique for detecting small metal particles (≤ 5 nm) or low metal contents (≤ 5) (Zieliński et al. 2005). In Fig. 3a, XRD pattern for the AC/NiO-7 shows the diffraction peaks at 2Θ = 37.3°, 43.29°, 62.87°, 75.42°, and 79.41° corresponding to (111), (200), (220), (311), and (222), respectively. Also, in Fig. 3b the AC/MgO-7 shows the diffraction peaks at 2Θ = 38.73°, 43.09°, 62.44°, 74.79°, and 78.73° corresponding to (111), (200), (220), (311), and (222), respectively. In Fig. 3a, it was envisaged that the size of the NiO crystallites on the carbon surface affected the pore structure and specific surface area. In the Ni–ACs, the metallic nickel peaks that are clearly found at 2Θ = 37.3°, 43.29°, and 62.87° were increasingly enhanced as the oxidation time increased (Jang and Park, 2012a, b). In Fig. 3b, all the samples except pure MgO display two broad peaks at around 44° and 63°, which were defined to the characteristic carbon (100) and (220) diffractions, respectively (Zhou et al. 2018). It seems that calcination of samples under N2 atmosphere caused to dissociation of nitrate hexahydrate since ($Ni(NO_3)2$ 0.6(H2O)) and ($Mg(NO_3)2$ 0.6(H2O)) were decomposed to NiO and MgO. It is worth noting that these peaks clearly became stronger and confirmed the results of previous works (Jang and Park 2012a, b; Zhou et al. 2018).

Figures 4 and 5 show the N_2 adsorption/desorption isotherms of AC, AC/NiO-3, and AC/MgO-3, and Table 3 presents the porous parameters of the adsorbents that have been modified by different weight percent of metals. All curves in Fig. 4 are fitted into the type IV isotherm and show a type B hysteresis loop, according to the International Union of Pure and Applied Chemistry (IUPAC) classification (Thommes et al. 2015). This type of isotherm is consistent with microporous and mesoporous materials. It was found that the raw ACs had the highest specific surface area, indicating that they were highly mesoporous. However, they decreased after the nickel and manganese electro less plating with the AC/NiO-3 and AC/MgO-3 sample due to the pore filling or blocking behaviors of the metallic coating.

A broad pore size distribution was obtained for the three adsorbents, as calculated by the BJH method in Fig. 5. However, after nickel oxide and magnesium oxide loadings, the pore structure was slightly decreased.

Specific surface area, total pore volume, total pore area, and pore size distribution for all samples, including AC and impregnated AC with different percentages of metal oxide, are shown in Table 2. Among all samples, the highest BET surface area belongs to the raw AC (962.74 m^2/g). Low metal oxide loading (1 wt%) is not very effective on the BET surface area or total pore area. However, Table 2 apparently shows decrease in the BET surface area and total pore area with increase in the percentage of metal oxide. Therefore, the structural properties and BET surface area depend on the amount of loaded metal oxide.

The last column of Table 2 shows the CO_2 adsorption capacity of proposed absorbents at 25 °C and 5 bar. AC is known as a porous material, and its high surface area causes higher adsorption capacity. The results showed that impregnation of AC with metal oxide reduces the BET surface area, but improves the adsorption capacity. These observations indicate that metal particles settled inside the AC pores and blocked the fine microporosity during impregnation. Adsorption of CO_2 does not only depend on the BET surface area and pore volume but also the reaction between adsorbate and adsorbent. A low metal loading limits the surface change, while the higher addition blocks microporous adsorbents and decreases the adsorption capacity. The experiments showed the highest adsorption capacity for AC/NiO-3 and AC/MgO-3. MgO impregnated samples exhibited a more significant reduction in specific surface area than

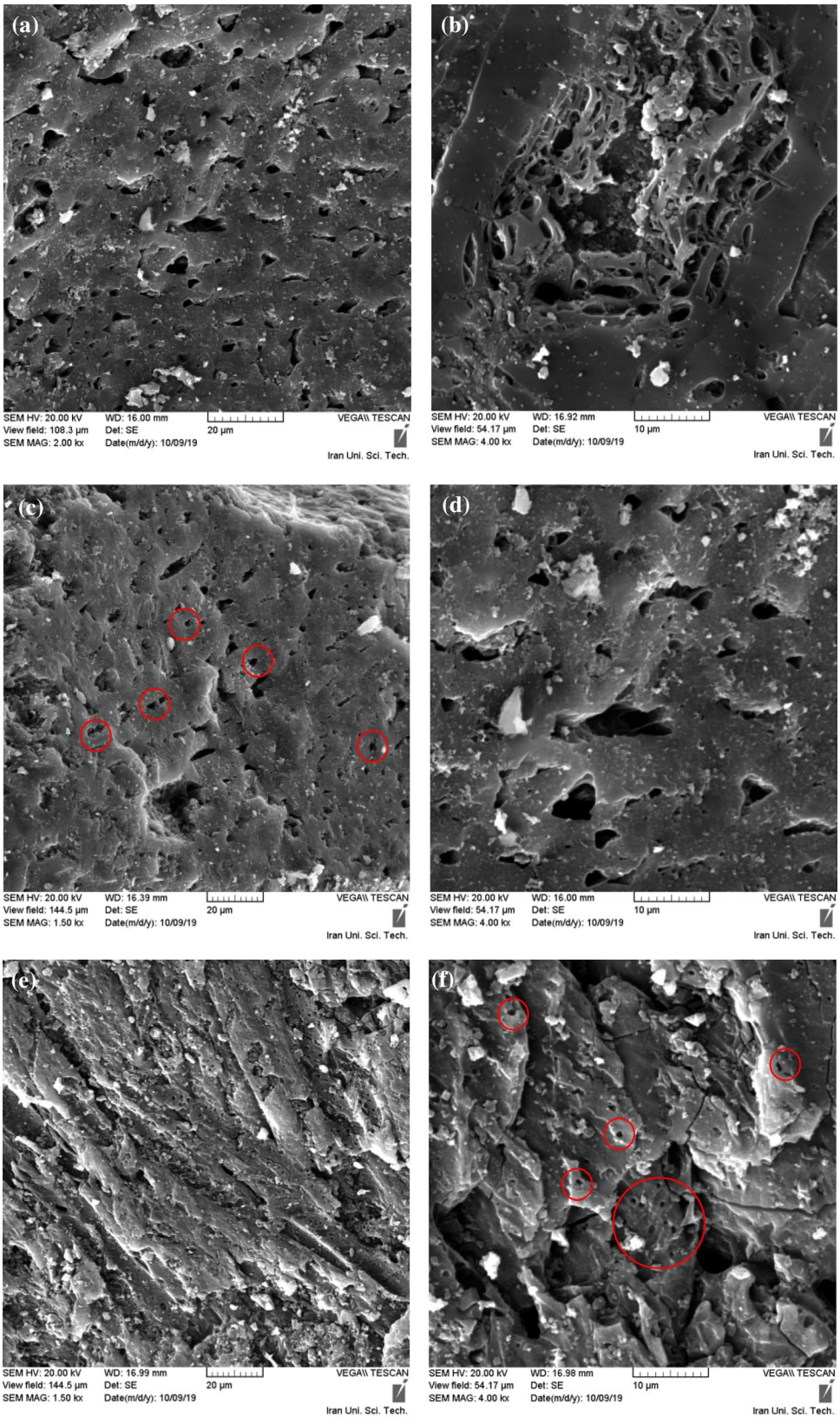

Fig. 2 SEM images of two scales including: **a** AC in 20.0 µm and **b** 10.0 µm, **c** AC/NiO-3 in 20.0 µm and **d** 10.0 µm and **e** AC/MgO-3 in 20.0 µm and **f** 10.0 µm

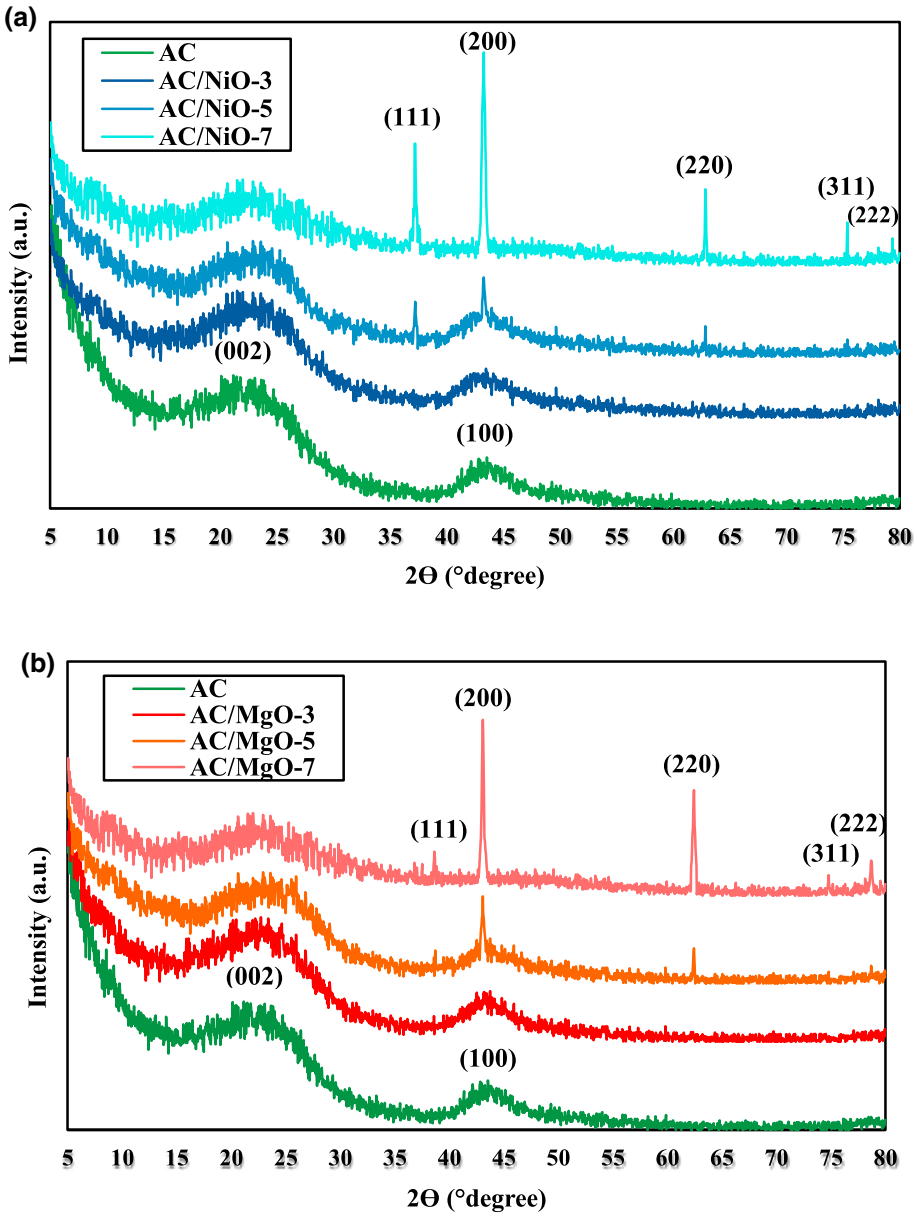

Fig. 3 X-ray diffraction analysis for **a** AC, AC/NiO-3, AC/NiO-5, AC/NiO-7 and **b** AC, AC/MgO-3, AC/MgO-5, AC/MgO-7

NiO, probably because of the larger molecular size of MgO (Jeffry D. Madura 1972). It may also block micropores, which can reduce the adsorption capacity.

RSM analysis

The design experiment and the responses have been investigated using RSM based on CCD method to optimize the CO_2 capture process on the modified AC adsorbents. The temperature, pressure, and absorbent type are three important factors that influence the design of experiments. Considering the five levels for each variable and a total of 39 runs, Table 3 shows the values of independent variables and their effects on the CO_2 adsorption capacity.

The analysis of variance (ANOVA) is a statistical tool to investigate the importance of the model, independent parameters, interactions, and second-order terms in the model. This analysis can be very helpful to obtain a satisfactory answer (Table 4). Two essential parameters for analyzing the design of the experiment are p value and F value. The model will be statistically significant, highly significant, and not significant at $p < 0.05$, $p < 0.001$, and $p > 0.1$, respectively, and if the model is more significant, the F value gets larger. R^2 further evaluates the performance of the model, adjusted R^2, predicted R^2, Adeq precision, and lack-of-fit parameters. High values of R^2 and nonsignificant ($P > 0.05$) indicate that this model is highly comparable with the results (Amiri et al. 2017; Ghaedi et al. 2019).

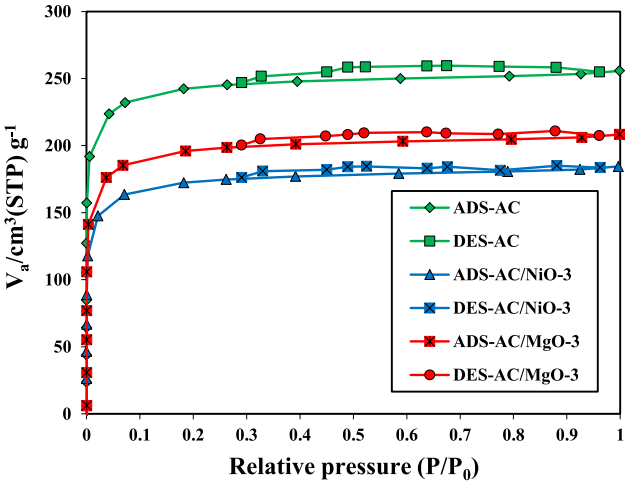

Fig. 4 Nitrogen adsorption/desorption isotherms of AC, AC/NiO-3, and AC/MgO-3

According to ANOVA, the F value and p value of the model are 490.48 and < 0.0001, respectively, which indicate that the model is significant. It means that there is only a 0.01% chance that this large F value could be due to noise. Also, A, B, C, AB, AC, BC, A^2, and B^2 are significant model terms. The F value of lack of fit is 2.62, so it is not significant relative to the pure error, and there is a 5.01% chance that the F value could be due to noise. The predicted R^2 value of 0.9674 and the adjusted R^2 value of 0.9930 have a difference of less than 0.2, so they are in a reasonable agreement. Adeq precision measures the signal-to-noise ratio, and the values greater than 4 is desirable. The ratio of 67.4315 shows that there are enough signals in the model that can be used to navigate the design space. The regression coefficient values were evaluated, and Eqs. (4–6) were obtained for adsorption capacity of AC, AC/NiO-3, and AC/MgO-3 as follow:

$$q_{AC} = 32.936 + 29.9563P - 1.2978T - 0.3358P.T - 0.3255P^2 + 0.0115T^2 \quad (4)$$

$$q_{AC/NiO-3} = 54.4484 + 39.2805P - 1.61095T - 0.33579PT - 0.3254 \times P^2 + 0.01151 \times T^2 \quad (5)$$

$$q_{AC/MgO-3} = 60.4979 + 34.5282P - 1.63037T - 0.33579PT - 0.3255P^2 + 0.01151T^2 \quad (6)$$

Equations (4–6) indicate the relationship between the adsorption capacity and the process parameters, which involve a constant coefficient, two first-order terms, one interaction term, and two second-order terms. The presented second-order polynomial models are suitable for the prediction of CO_2 adsorption capacity and show a reasonably good agreement with the quadratic model.

Two diagnostic plots, including normal probability plot and predicted values vs. actual values, are illustrated in Fig. 6a, and b, respectively, to test the ANOVA assumptions. Since the error values in Fig. 6a are very close to the straight line; the assumption of normal distribution of error is reasonable. Errors are defined as the difference between the actual values and the predicted values. Figure 6b obviously shows that the differences between predicted values and actual values are trivial, so the models are very predictive and can fit the data well. It suggests that the CO_2 adsorption process can be accurately analyzed and optimized by the proposed models.

Externally studentized residuals versus predicted adsorption capacity are shown in Fig. 7a. This figure shows that

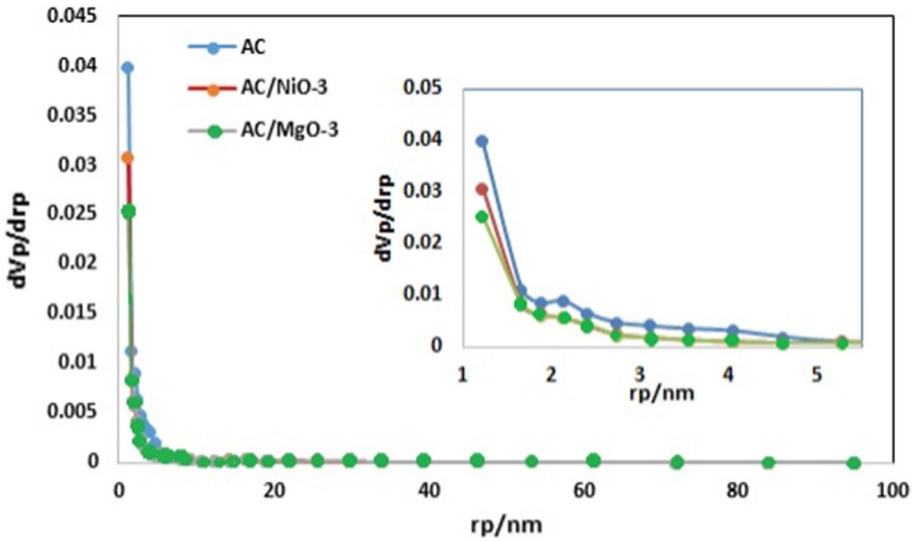

Fig. 5 Pore size distributions of AC, AC/NiO-3, and AC/MgO-3

Table 2 The structural properties, BET analysis, and adsorption of adsorbents at 5 bar

Samples	S_{BET}[a] ($m^2\ g^{-1}$)	V_t[b] ($cm^3\ g^{-1}$)	V_p[c] ($cm^3\ g^{-1}$)	Micropore area[d] ($m^2\ g^{-1}$)	The average pore diameter[e] (nm)	Adsorption at 25 °C (mg/g)
AC	962.74	0.4031	0.041585	50.305	1.7078	109.23
AC/NiO-1	960.92	0.4021	0.041179	49.913	1.6913	120.15
AC/NiO-3	924.44	0.3836	0.039017	48.106	1.6598	171.84
AC/NiO-5	813.51	0.3376	0.034328	42.481	1.5982	149.51
AC/NiO-7	691.48	0.2903	0.029864	36.958	1.3901	104.66
AC/MgO-1	957.51	0.4006	0.409837	49.593	1.6938	117.97
AC/MgO-3	819.93	0.3437	0.036104	42.963	1.6363	154.32
AC/MgO-5	713.34	0.3024	0.031771	40.854	1.4895	138.88
AC/MgO-7	599.85	0.2731	0.027645	35.543	1.2956	99.87

[a]Obtained by BET measurement

[b]The total hole volume. MP-plot method

[c]Calculated by the BJH (desorption) method using N_2 adsorption isotherm

[d]Obtained by the t-plot method

[e]Obtained by the MP-plot method

there is no need to assume any violation of independence, and the plot should follow a random distribution. In addition, they have no apparent patterns and unusual structures. It can be concluded that the models are satisfactory, and there is no reason to suspect any infringement of independence or assumption of continuous variables. The DFFITS plot for adsorption capacity in Fig. 7b is a measure of the influence of each point on the predicted value. It can be seen that all data have been located in the specified range between blue lines, which indicate the reliability of the model.

Effect of model parameters and interactions

To detect and optimize reaction conditions, 3D response surfaces, which are a graphical representation of the regression equation, are a good choice. These plots determine the response functions for two parameters. In contrast, all other parameters are constant at the response levels and have a beneficial impact on realizing the direct and interaction effects of these variables. Figure 8 illustrates the interaction between two variables and their effects on the CO_2 adsorption capacity.

Temperature and pressure effects on adsorption capacity

In this study, some experiments have been designed to express the effect of temperature and pressure on CO_2 adsorption other than RSM experiments to confirm the results. Figure 9 shows the CO_2 adsorption capacity at a constant pressure of 5 bar and different temperatures of 25, 40, 55, 70, and 85 °C. As expected, the adsorption capacity decreased with rise in temperature. CO_2 adsorption is an exothermal process, and when the temperature increases, the molecule's speed also increases, and fewer molecules can adsorb on the adsorbent (Hosseini, et al. 2015). The temperature has not the same effect on the adsorption capacity of raw AC and AC modified with nickel oxide and magnesium oxide.

In the CO_2 adsorption process, the empty pores of AC are easily filled with a monolayer CO_2, followed by multilayer CO_2. After metal impregnation, the AC pores are filled with NiO and MgO, and the metals are linked to the functional groups of AC. Although the pore volume decreases, the adsorption capacity increases. In raw AC, the only physisorption occurs, and the adsorption capacity sharply decreases at higher temperatures. But in the case of metal impregnated AC, CO_2 reacts with the oxygen agents of metal oxide, and both chemisorption and physisorption occur. Therefore, with increase in temperature, the adsorption capacity decreases to a lesser extent. For example, by raising the temperature from 25 to 85 °C, the adsorption capacity of raw AC reduced by 96%, but 72% and 77% for AC/NiO-3 and AC/MgO-3, respectively.

Another set of experiments have been done at a constant temperature of 25 °C and different pressures of 2, 4, 6, 8, and 10 bar (Fig. 10). The results indicated that the pressure has a positive effect on the adsorption capacity, independent of the type of adsorbent and physical or chemical adsorption (Taheri et al. 2019). The gas molecules get compressed and packed together more tightly at higher pressures. Besides, more molecules have a higher chance to be adsorbed on available sites, so the number of adsorbed molecules increases (Plaza et al. 2010). The importance of pressure and its effect on the adsorption capacity was proved by analysis of variance.

Table 3 Experimental values of the design and response of adsorption experiments in impregnated AC

Std	Run	A (P) bar	B (T) °C	C adsorbent	q mg/g
15	1	7.8	33.0	AC/NiO-3	198.250
32	2	9.0	52.5	AC/MgO-3	128.231
16	3	2.2	72.0	AC/NiO-3	27.518
5	4	1.0	52.5	AC	13.340
4	5	7.8	72.0	AC	25.540
33	6	5.0	25.0	AC/MgO-3	154.314
31	7	1.0	52.5	AC/MgO-3	28.953
9	8	5.0	52.5	AC	50.985
11	9	5.0	52.5	AC	42.824
25	10	5.0	52.5	AC/NiO-3	103.025
19	11	9.0	52.5	AC/NiO-3	168.365
23	12	5.0	52.5	AC/NiO-3	98.692
20	13	5.0	25.0	AC/NiO-3	171.840
39	14	5.0	52.5	AC/MgO-3	83.029
35	15	5.0	52.5	AC/MgO-3	84.029
12	16	5.0	52.5	AC	52.762
26	17	5.0	52.5	AC/NiO-3	106.887
27	18	2.2	33.0	AC/MgO-3	61.312
17	19	7.8	72.0	AC/NiO-3	101.654
7	20	5.0	25.0	AC	109.222
2	21	7.8	33.0	AC	135.140
13	22	5.0	52.5	AC	48.136
22	23	5.0	52.5	AC/NiO-3	99.254
18	24	1.0	52.5	AC/NiO-3	27.570
29	25	2.2	72.0	AC/MgO-3	21.133
10	26	5.0	52.5	AC	47.106
8	27	5.0	80.0	AC	11.994
37	28	5.0	52.5	AC/MgO-3	85.638
36	29	5.0	52.5	AC/MgO-3	83.547
3	30	2.2	72.0	AC	10.719
6	31	9.0	52.5	AC	80.880
38	32	5.0	52.5	AC/MgO-3	81.929
14	33	2.2	33.0	AC/NiO-3	68.959
1	34	2.2	33.0	AC	38.262
28	35	7.8	33.0	AC/MgO-3	180.785
24	36	5.0	52.5	AC/NiO-3	106.124
21	37	5.0	80.0	AC/NiO-3	50.871
34	38	5.0	80.0	AC/MgO-3	31.240
30	39	7.8	72.0	AC/MgO-3	72.357

As a result, the values of the adsorption capacity are consistent with the model outputs, which shows the reliability of the model in probing the variable effects on the adsorption capacity. The effect of AC surface modification on CO_2 adsorption capacity at different temperatures and pressures is summarized in Fig. 11a, b.

Adsorption isotherm

The adsorption isotherms at 25 °C and pressure range of 2–10 bar for AC, AC/NiO-3, and AC/MgO-3 are shown in Fig. 12. Adsorption isotherms describe the equilibrium of chemical or physical adsorption on the solid material surface at various pressures and constant temperature. The adsorption isotherm plays a key role in optimizing the used adsorbents and a description of the interaction between the adsorbate and the adsorbent. In the current study, the CO_2 adsorption data on AC, AC/NiO-3, and AC/MgO-3 were fitted to standard isotherm models such as Langmuir, Freundlich, Dubinin–Radushkevich (D-R), and Spis models. The Langmuir model was initially created for adsorption of gas on solid, and the results showed that the adsorption occurs in the absence of any interaction between the adsorbed molecules, and there is a single-molecular-layer arrangement on the adsorbent surface. The simple Langmuir isotherm model is (Langmuir 1916):

$$\frac{P_{CO_2}}{q_e} = \frac{1}{K_L.q_m} + \frac{P_{CO_2}}{q_m} \tag{7}$$

where q_e (mg/g), q_m (mg/g), P_{CO2} (bar), and K_L (1/bar) are the equilibrium adsorbed quantity, the maximum adsorption capacity, the gas pressure in equilibrium, and Langmuir constant, the basic properties of the Langmuir isotherm can be declared regarding separation factor (R_L). Equation (8) is the definition of this dimensionless parameter:

$$R_L = \frac{1}{1 + K_L P_0} \tag{8}$$

Where P_0 (bar) is the initial adsorbate pressure. The type of isotherm depends on the R_L values: unfavorable ($R_L > 1$), linear ($R_L = 1$), favorable ($0 < R_L < 1$), and irreversible ($R_L = 0$) (Das, et al. 2013).

The Freundlich isotherm is an experiential equation used to describe heterogeneous systems (Hameed, et al. 2009). In this model, the adsorbent molecules form a mono- or multilayer on the surface of the heterogeneous adsorbent. Freundlich model can be expressed linearly as Eq. (9) (Freundlich 1907):

$$\ln q_e = \frac{1}{n} \ln(P_{CO_2}) + \ln(K_f) \tag{9}$$

where K_f ((bar^n.mg)/g) is related to the adsorption capacity and n describes the adsorption affinity and heterogeneity of the surface. The 1/n value less than one ($0 < n < 1$) indicates optimal adsorption. D-R adsorption equation can be used for a large number of micropores in the microporous adsorbent (Fashi et al. 2019). The D-R equation is:

Table 4 ANOVA results for RSM-CCD model of the second-order polynomial model of adsorption capacity

Source	Sum of squares	df	Mean square	F value	*p* value
Model	97,260.43	11	8841.86	490.48	< 0.0001
A-P	36,060.95	1	36,060.95	2000.40	< 0.0001
B-T	35,694.49	1	35,694.49	1980.07	< 0.0001
C- Adsorbent	17,809.84	2	8904.92	493.98	< 0.0001
AB	4093.03	1	4093.03	227.05	< 0.0001
AC	2782.42	2	1391.21	77.17	< 0.0001
BC	210.70	2	105.35	5.84	0.0078
A2	141.49	1	141.49	7.85	0.0093
B2	395.45	1	395.45	21.94	< 0.0001
Residual	486.73	27	18.03		
Lack of fit	372.71	15	24.85	2.62	0.0501
R2 = 0.995	Adjusted R2 = 0.993		Predicted R2 = 0.967	Adeq precision = 67.431	

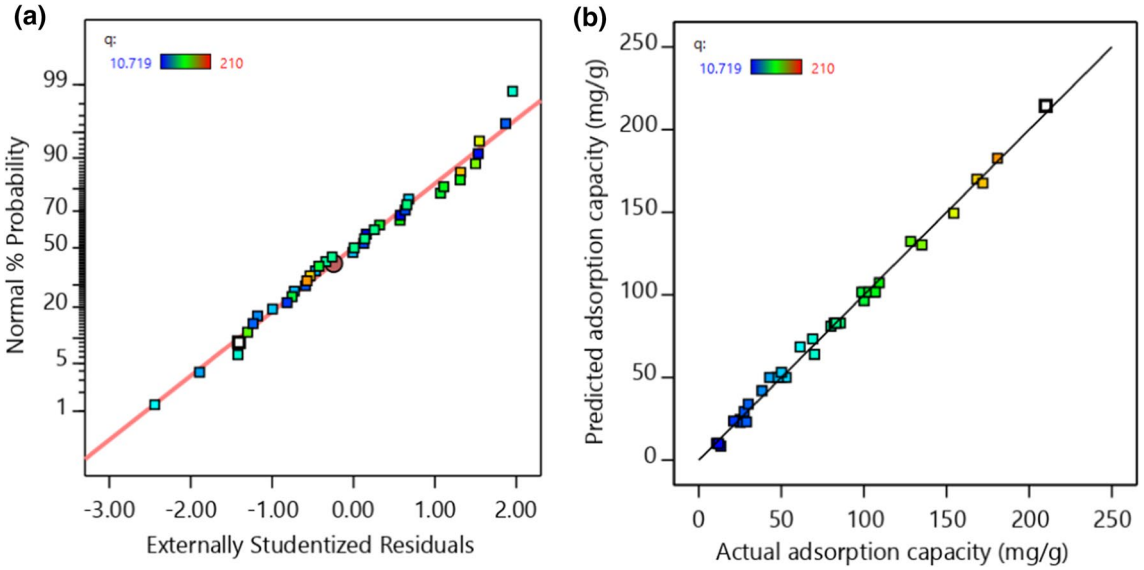

Fig. 6 Diagnosis of the model, **a** normal plot of residuals **b** the predicted adsorption capacity values vs. the actual values of adsorption capacity

$$\ln q_e = \ln q_m - \beta \cdot \varepsilon^2 \tag{10}$$

$$\varepsilon = \mathrm{RT} \ln \left[1 + \frac{1}{P_{\mathrm{CO}_2}} \right] \tag{11}$$

$$E_a = \frac{1}{\sqrt{2\beta}} \tag{12}$$

where β (mol^2/KJ^2) is D-R constant related to the mean sorption free energy, and ε (KJ^2/mol^2) is Polanyi potential, which is the amount of energy required for separation of an adsorbent from the adsorbent surface. In order to better describe the heterogeneous surface, Sips isotherm model (Sips 1948) as a combination of the Langmuir and Freundlich isotherm models was suggested. This isotherm approaches the Freundlich isotherm and Langmuir isotherm, at low and high adsorbent concentrations, respectively (Ahmed and Dhedan 2012). The Sips equation is defined as follows:

$$\beta_S \ln(C_e) = -\ln\left(\frac{K_S}{q_e}\right) + \ln a_S \tag{13}$$

where K_S (L.g^{-1}), β_s, and a_s (L.mg^{-1}) are Sips isotherm model constant related to the energy of adsorption, Sips isotherm model exponent, and Sips isotherm model constant, respectively.

Isotherm parameters obtained from the curve fitting of various models are given in Table 5. According to R^2 parameters reported in Table 5, the results show that the Freundlich isotherm has better results than the

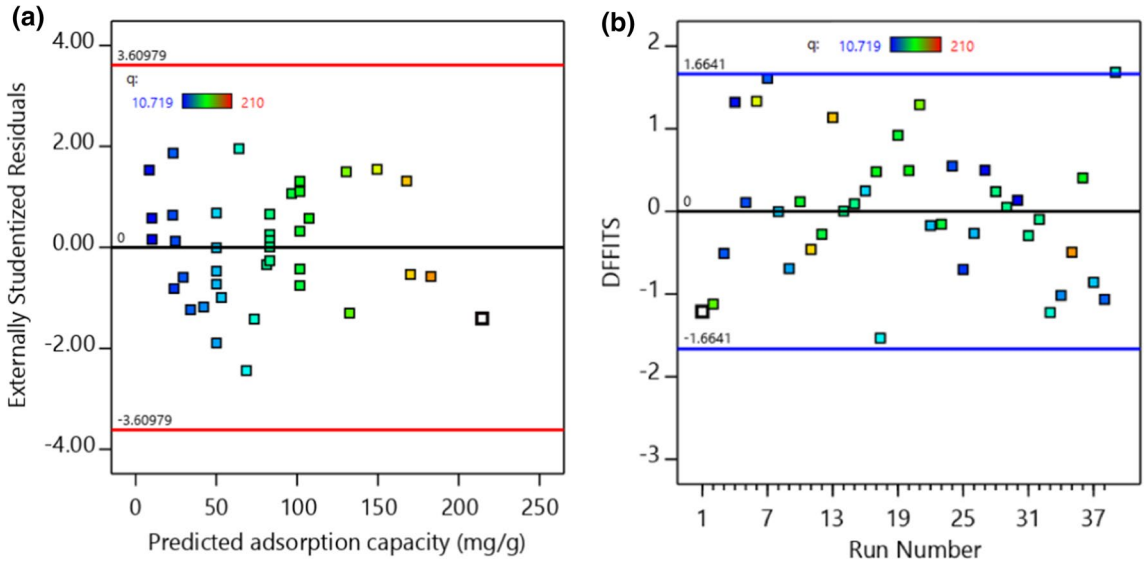

Fig. 7 Diagnosis of the model, **a** externally studentized residuals vs. predicted adsorption capacity, **b** difference in fits (DFFITS) plot for evaluating of the quadratic model

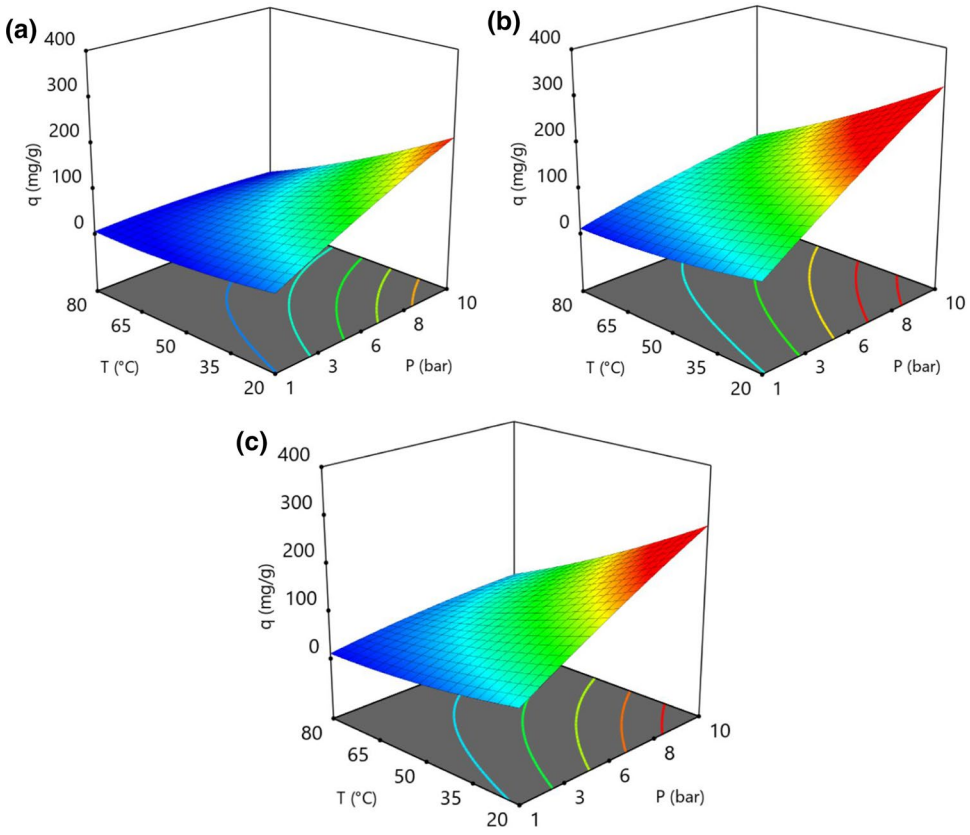

Fig. 8. 3D response surfaces and 2D contour plots for determination of interactions between P and T and their impacts on CO_2 adsorption capacity (q) for **a** AC, **b** AC/NiO-3, and **c** AC/MgO-3

other isotherms for raw AC. This model represents multilayer adsorption, and since in raw AC carbon multilayer adsorption is performed by the physical adsorption mechanism, the Freundlich model is the most suitable. The sips isotherm, which is a combination of the Langmuir and Freundlich isotherms, fits well with the experimental data, especially for AC/NiO-3 and AC/MgO-3 adsorbents. In addition, after the Sips model, the Langmuir model, which is the best description of the chemical reaction due to being limited to one layer, is the appropriate model.

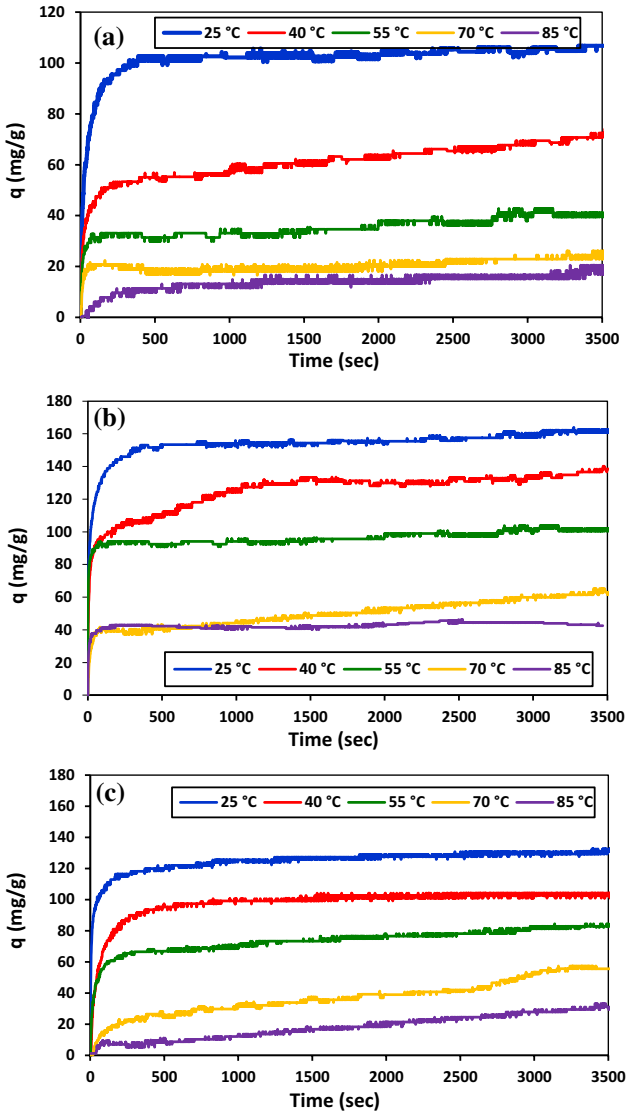

Fig. 9 Experimental CO_2 adsorption capacity by **a** AC **b** AC/NiO-3 **c** AC/MgO-3 at a constant pressure of 5 bar and different temperatures of 25, 40, 55, 70, and 85 °C

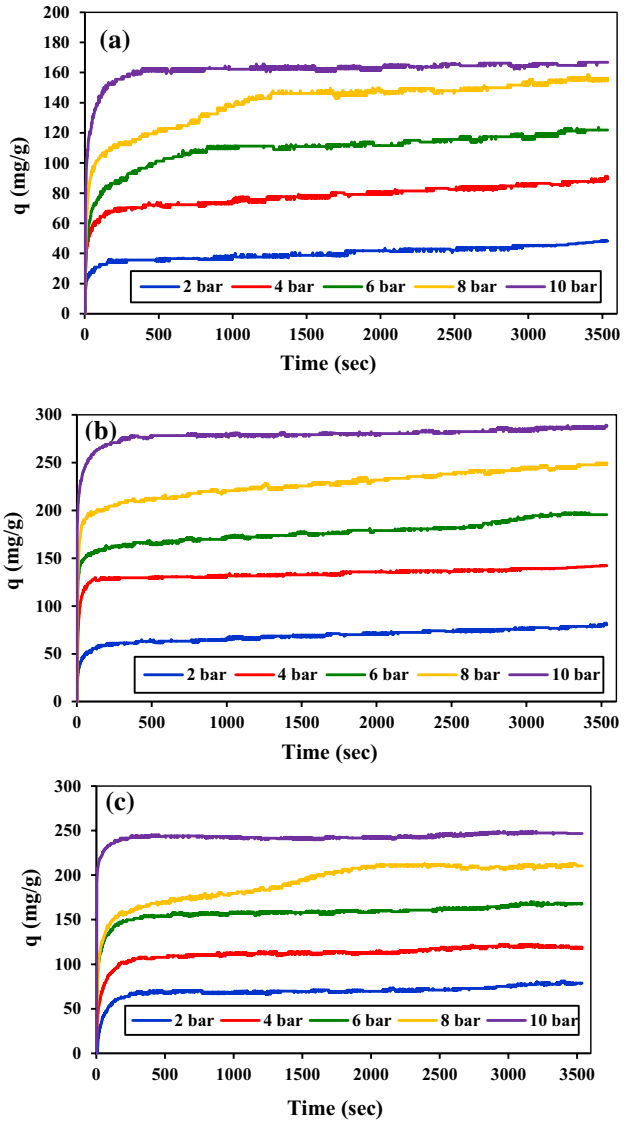

Fig. 10 Experimental CO_2 adsorption capacity by **a** AC **b** AC/NiO-3 **c** AC/MgO-3 at a constant temperature of 25 °C and different pressures of 2, 4, 6, 8, and 10 bar

The capability of Langmuir, Freundlich, D-R, and Sips isotherms is compared in Fig. 13.

Adsorption kinetic

The adsorption data can be applied on different adsorption kinetic models, including chemical reaction models (first-order and second-order kinetic models), mass transfer model (Olivitch equation), and velocity control equation to determine the CO_2 adsorption mechanism on the adsorbent (Khajeh Amiri et al. 2019). The Lagergren first-order rate equation (Lagregren 1898) is as follows:

$$\log\left[q_e - q_t\right] = \log q_e - \frac{K_1}{2.303} * t \tag{14}$$

where q_e ($mg.g^{-1}$), q_t ($mg.g^{-1}$), t (min), and K_1 (min^{-1}) are the equilibrium adsorption capacity, adsorption capacity, time, and rate constant. Ho (Ho and McKay 1999) expressed the second-order kinetic model based on the sorption capacity of the solid phase, as can be seen in Eq. (15):

$$\frac{t}{q_t} = \frac{1}{K_2 * q_e^2} + \frac{t}{q_e} \tag{15}$$

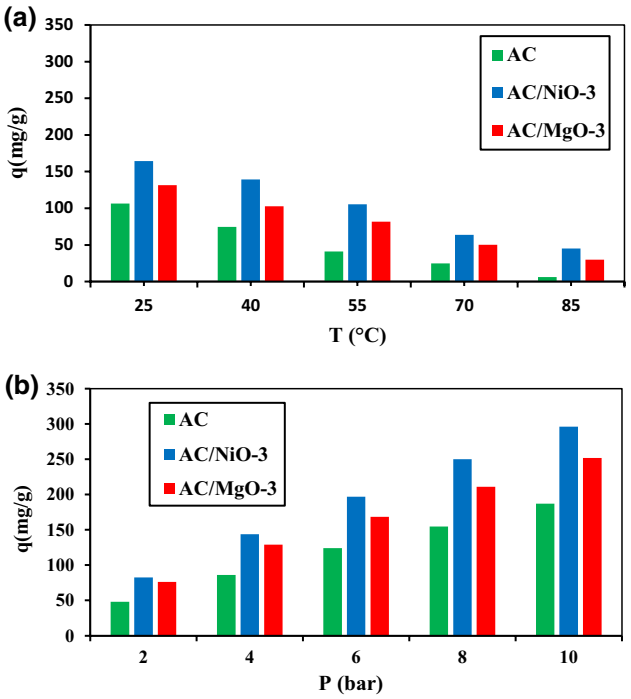

Fig. 11 Effect of surface modification of AC on adsorption capacity at different **a** temperatures and **b** pressures

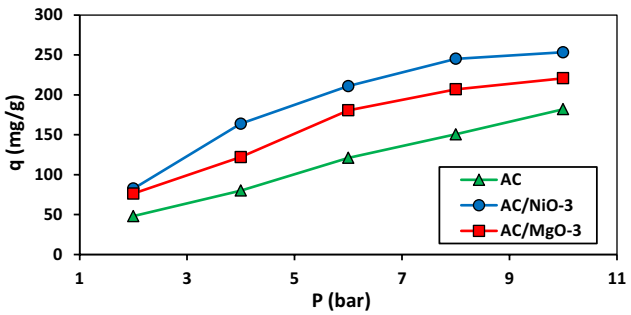

Fig. 12 Experimental data for CO_2 adsorption isotherm in AC, AC/NiO-3, and AC/MgO-3 adsorbent

where K_2 ($g.mg^{-1}.min^{-1}$) is the rate constant. By sketching a graph of t/q_t based on t and finding the slope and intercept, the second-order parameters can be extracted.

The Elovich model (Aharoni and Tompkins 1970) is generally applied to specify the chemical adsorption of gases on heterogeneous solids (Eq. (16)).

$$q_t = \beta \cdot \log(\alpha \cdot \beta) + \beta \cdot \log(t) \quad (16)$$

Table 5 Parameters of the adsorption isotherm model for raw and modified AC

Model	Parameter	AC	AC/NiO-3	AC/MgO-3
Langmuir	q_m	806.813	469.205	444.625
	K_L	0.029	0.128	0.104
	R^2	0.989	0.998	0.992
Freundlich	K_F	25.843	66.875	52.613
	n	1.179	1.652	1.556
	R^2	0.999	0.976	0.986
D-R	q_m	183.534	264.777	225.249
	E_a	0.492	0.632	0.618
	β	2.063	1.253	1.310
	R^2	0.983	0.991	0.988
Spis	K_s	25.818	34.98	39.079
	β_s	0.850	1.687	1.235
	A_s	0.001	0.116	0.123
	R^2	0.987	0.999	0.993

In Eq. (16), α ($mg.g^{-1}.min^{-1}$) is the initial adsorption rate, and β parameter ($g\ mg^{-1}$) is related to the surface coverage and activation energy for chemical adsorption.

The adsorption process on porous solids involves three stages, including mass transfer (boundary layer/film diffusion), ions adsorption onto sites, and intraparticle diffusion inside the pore. It is very likely that the intraparticle diffusion will be the rate-limiting step, and it is considered as a rate controlling model (Eq. (17)).

$$q_t = K_{id}.t^{0.5} \quad (17)$$

where K_{id} is the intraparticle diffusion coefficient in the adsorption process, which can be obtained by plotting the qt versus $t^{0.5}$. Table 6 presents the parameters of the kinetic models.

The R^2 values of raw AC samples, it became clear that the first-order kinetic model provides the best CO_2 capture data. In general, the first-order model can be an indication of reversible interaction between the adsorbent and absorbable gas, which is appropriate for the prediction of physical adsorption behavior. It was found that the Elovich and second-order models provide better results for the adsorption on the AC modified with NiO and MgO, maybe because the CO_2 molecules bind to the modified AC by the formation of a chemical bond. Figure 14 presents the experimental data and kinetic models for CO_2 adsorption on AC, AC/NiO-3, and AC/MgO-3 at 5 bar and 25 °C.

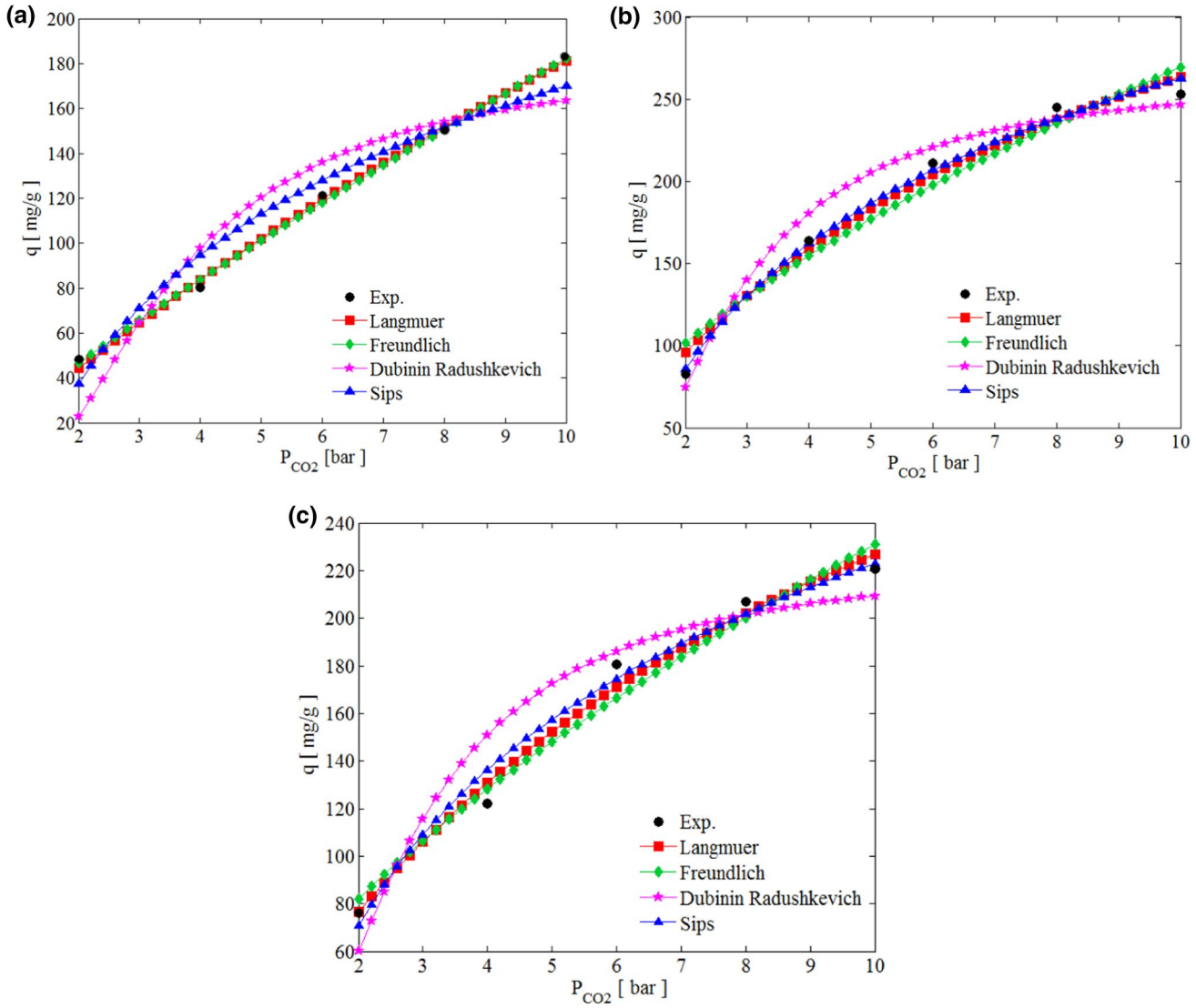

Fig. 13 Comparison of isotherms and CO_2 adsorption experimental data by **a** AC **b** AC/NiO-3 **c** AC/MgO-3 at 25 °C

Table 6 Parameters of kinetic models for CO_2 adsorption by raw and modified AC adsorbent

Kinetic model	Parameter	AC			AC/NiO-3			AC/MgO-3		
		25 °C	55 °C	85 °C	25 °C	55 °C	85 °C	25 °C	55 °C	85 °C
First-order	q_e	102.709	35.275	15.499	153.278	93.763	60.902	119.581	74.653	41.179
	K_1	0.024	0.043	0.003	0.048	0.139	0.121	0.069	0.023	0.108
	R^2	0.990	0.958	0.985	0.877	0.804	0.987	0.896	0.949	0.945
Second-order	q_e	105.904	36.531	18.177	156.963	97.850	62.278	124.437	77.286	43.059
	K_2	0.003	0.002	0.005	0.001	0.002	0.004	0.001	0.001	0.004
	R^2	0.911	0.921	0.968	0.926	0.938	0.986	0.965	0.989	0.973
Elovich	alfa	0.128	4.302	0.018	13.146	16.574	0.017	82.284	0.130	0.815
	beta	13.259	3.661	3.136	12.813	4.1	4.051	9.111	10.036	2.445
	R^2	0.957	0.882	0.982	0.989	0.834	0.983	0.969	0.974	0.815
Rate controlling	k_{id}	2.455	0.883	0.332	3.875	2.407	0.468	3.083	1.807	1.07
	R^2	0.832	0.765	0.959	0.905	0.564	0.983	0.844	0.877	0.631

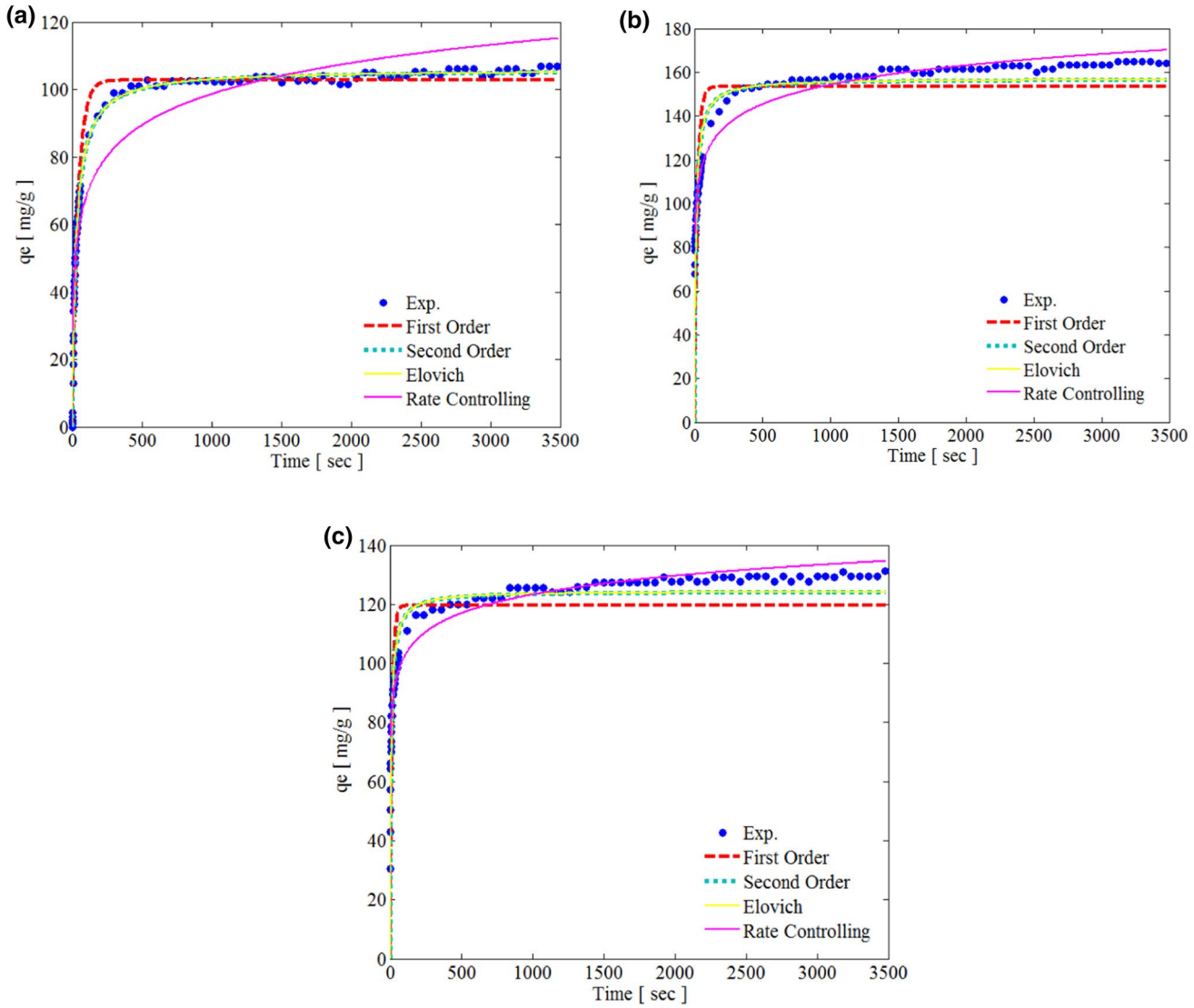

Fig. 14 Experimental data and kinetic models for CO_2 adsorption by **a** AC **b** AC/NiO-3 **c** AC/MgO-3 at 5 bar and 25 °C

Adsorption thermodynamic

The enthalpy change (ΔH°), Gibbs free energy change (ΔG°), and entropy change (ΔS°) are the most important thermodynamic properties that can be estimated by temperature-changing equilibrium constants. The entropy and Gibbs free energy values are very useful for the determination of the spontaneity of the process (Adelodun et al. 2016). Equations (18) and (19) are well-known thermodynamic equations for calculation of equilibrium constant (K_d) and ΔG° parameters:

$$\ln K_d = \frac{\Delta S^o}{R} - \frac{\Delta H^o}{RT} \tag{18}$$

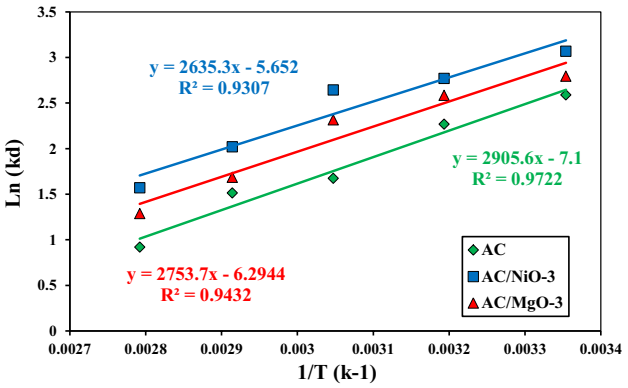

Fig. 15 Plot of Ln (k_d) vs. 1/T for CO_2 adsorption by **a** AC, **b** AC/NiO-3, and **c** AC/MgO-3 at 5 bar and 25 °C

Table 7 Thermodynamic parameters of CO_2 adsorption on AC, AC/NiO-3, and AC/MgO-3 adsorbents at 5 bar

Absorbent sample	ΔH°	ΔS°	ΔG° (kJ/mol)				
	(kJ/mol)	(kJ/mole K)	298	313	328	343	358
AC	−24.158	−0.059	−6.558	−5.672	−4.787	−3.901	−3.016
AC/NiO-3	−21.911	−0.047	−7.900	−7.195	−6.490	−5.785	−5.080
AC/MgO-3	−22.896	−0.052	−7.292	−6.507	−5.722	−4.937	−4.152

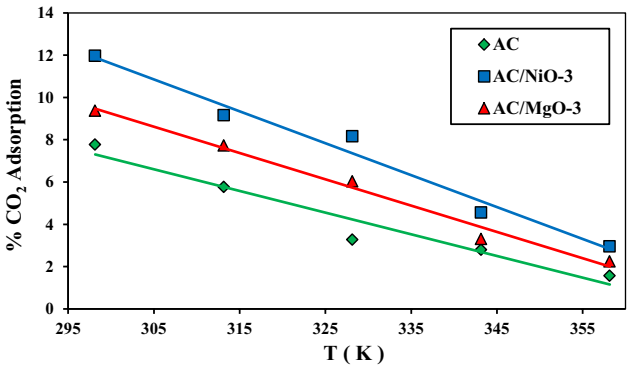

Fig. 16 Plot of CO_2 adsorption percentage of different adsorbents vs. temperature at 5 bar

Table 8 Adsorption optimization of the CO_2 adsorption by AC/NiO-3 and AC/MgO-3

Parameter and response	Constrain	Low	High	Optimum condition	
				AC/NiO-3	AC/MgO-3
P (bar)	In range	1.0	9.0	7.8	7.8
T (°C)	Maximize	33.0	72.0	62.7	57.1
q (mg/g)	Maximize	10.72	210	121.35	105.17

$$\Delta G^\circ = \Delta H^\circ - T\Delta S^\circ \tag{19}$$

The slope and intercept of a curve of ln (K_d) based on (1/T) have corresponded to the ΔH° and ΔS° values, respectively (Fig. 15). All calculated thermodynamic properties are summarized in Table 7.

According to Table 7, ΔH° values of CO_2 adsorption on the raw AC and modified AC are negative in the temperature range of 25–80 °C. It means that the process is exothermic, and the energy is released during the adsorption. ΔH° value of AC (−24.158 kJ/mol) reduces after loading of NiO (−21.911 kJ/mol) and MgO (−22.896 kJ/mol), so modified AC adsorbents release lower energy than AC in the adsorption process. By decreasing the degree of freedom, entropy decreases during the adsorption process, and a negative value of ΔS° is obtained. ΔG° is negative for all systems at different temperatures, so the process can proceed spontaneously and is thermodynamically favorable. ΔG° is less negative at higher temperatures, so there is a low driving force for proceeding the adsorption and a low tendency for adsorbent to adsorb at higher temperatures. Figure 16 illustrates the effect of temperature on the CO_2 adsorption at 5 bar pressure.

Optimal conditions

In this section, the best conditions have been detected to enhance the adsorption capacity of modified AC adsorbents. The process was optimized using the numerical optimization section in Design Expert software. It should be mentioned that every input parameter in Table 8 has been defined at a specific range, and therefore, the regression models are valid only in these ranges. Each parameter can be used in the range, maximum, minimum, target, and none (for responses) to obtain an optimum output for a set of conditions. In the current work, the reactor pressure was chosen in the design range for AC modified with NiO and MgO to reach a maximum response. To reach the highest efficiency for the adsorbent under flue gas conditions, the maximum values of temperature and q in the design range are selected. According to Table 8, the best adsorption capacity of 121.35 mg/g was obtained for AC/NiO-3 adsorbent at 62.7 °C and 7.8 bar. In addition, the response value of AC/MgO-3 adsorbent was 105.17 mg/g at 57.1 °C and 7.8 bar. Figure 17 shows the contour graph for the adsorption capacity of AC/NiO-3 and AC/MgO-3 at optimal conditions.

Comparison of various AC impregnated with metals

Table 9 compares the maximum CO_2 adsorption on AC impregnated with metals in this work with some different AC impregnated adsorbents previously used for CO_2 capture. As observed, the maximum CO_2 adsorption capacities

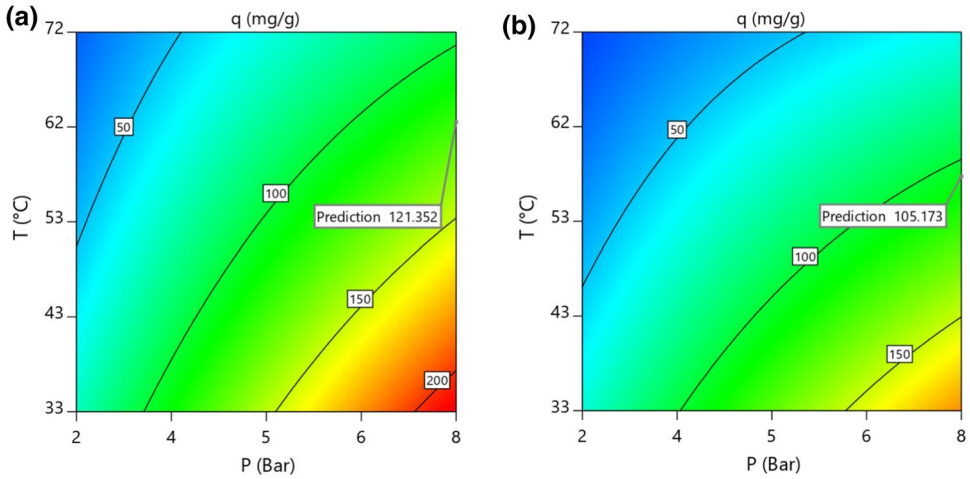

Fig. 17 Contour graph for adsorption capacity of **a** AC/N−iO-3 and **b** AC/MgO-3 at optimal conditions

Table 9 Comparison of the maximum CO_2 adsorption various AC impregnated with metals

Adsorbent	Modification process	BET surface area (m^2/g)	T (°C)	P (bar)	CO_2 (%)	Adsorption capacity (mmol/g)	Ref.
Commercial AC (Norit SA2)	Untreated	1316	30–50	1–2	5–50	0.58–4.09	(Hosseini, et al. 2015)
	HNO_3 treatment-Cu/Zn impregnation	599–1195				1.64–2.26	
Coconut shell AC	Untreated	1344	–	–	100	0.27	(Yi, et al. 2014)
	Cu, Ca, Mg, Zn impregnation	1339				0.326–0.367	
Commercial AC	Untreated	–	30	–	0.25	0.652	(Fenrong, et al. 2010)
	Cu, Ce impregnation					0.856	
Charcoal AC	Untreated	863	25	–	100	2.617	(Hakim, et al. 2015)
	Fe impregnation	487				2.356	
Charcoal AC	Untreated	1608	25	1	100	1.684	(Jang and Park 2012a, b)
	HNO_3 treatment-Ni impregnation	1053				2.039	
Charcoal AC (GR MERCK)	Untreated	1011	20–100	–	100	1.4–2.2	(Carabineiro, et al. 2001)
	Mg, Ba, Pb, Cu, Fe impregnation	–				0.4–4.6	
Coconut char AC	Untreated	277	25	1–7	–	1.091	(Son et al. 2005)
	Mg, Ca, Cu, Co, Ni impregnation	242–519				0.387–2.204	
Carbon-based adsorbent (MSC-30, GO8H)	Untreated	2250–3370	300	1	100	0.13–0.17	(Yong et al. 2001)
	Mg, Ca, Cu, Co, Ni impregnation	1272–1635				0.22–0.28	
Commercial AC (Norit RB3)	Untreated	959	25–95	0.3–1.1	100	0.3–1.2	(Somy et al. 2009)
	Cr, Fe/Zn impregnation	541–951				0.01–1.5	
Commercial AC (Mahab zist)	Untreated	962.74	25–85	2–10	100	0.1–3.88	This work
	NiO/MgO impregnation	925–820				5.9/5.1	

of AC-MgO and AC-NiO are much higher than that of many other previously reported adsorbents, indicating the promising application of AC–MgO and AC-NiO to be an effective adsorbent for CO_2 capture.

Conclusion

The CO_2 adsorption capacity and experimental modeling were studied on AC modified with NiO and MgO at different pressures and temperatures. The optimum

concentration of nickel nitrate and magnesium nitrate was obtained at 3 wt%. In this condition, the BET surface area of AC was decreased from 962.74 (m^2/g) to 924.44 (m^2/g) and 819.93 (m^2/g) in the presence of nickel nitrate and magnesium nitrate, respectively. By impregnation of AC adsorbent with nickel nitrate and magnesium nitrate, the CO_2 adsorption capacity increased by 57% and 41%, respectively, at 25 °C and 5 bar. XRD pattern of the originally activated carbons (AC-0), AC–MgO, and AC-NiO composites is displayed two broad peaks. The results showed that nickel nitrate and magnesium nitrate loaded on the AC surface was properly converted to the oxide in the calcination process. To optimize the operational conditions and adsorbent properties of raw and modified AC, 39 tests were designed with RSM. The best adsorption capacity of 121.35 mg/g was obtained for AC/NiO-3 absorbent at 62.7 °C and pressure 7.8 bar, under the flue gas condition. The AC/MgO-3 adsorbent also showed a response of 105.17 mg/g at 57.1 °C and 7.8 bar, as optimum conditions. The maximum adsorption capacities were found to be 5.9 mmol/g and 5.1 mmol/g at 10 bar and 25 °C for AC/NiO-3 and AC/MgO-3 absorbents, respectively. The study of isotherm models showed that the Freundlich model is better for the description of raw AC due to physical adsorption, and the Langmuir and Sips model are well fitted to modified AC due to single-layer adsorption. From the kinetic models, the second-order and Elovich models were fitted well to the modified adsorbents with high surface energy, because of the chemical bond formation between CO_2 molecule and modified AC. On the other hand, thermodynamic studies confirmed the negative values of $\Delta H°$ for modified AC, which lead to a decrease in the energy released in the adsorption process. In addition, $\Delta G°$ was less negative with increase in temperature, which indicates the lower tendency of the adsorbent for the adsorption process.

Declarations

Conflict of interest The authors declare that they have no conflict of interest.

References

Adamski A et al (2007) Surface modification of ZrO_2 nanopowder with oxovanadium species using slurry deposition and impregnation methods. J Alloy Compd 442(1–2):302–305

Adelodun AA et al (2016) Isotherm, thermodynamic and kinetic studies of selective CO_2 adsorption on chemically modified carbon surfaces. Aerosol Air Qual Res 16:3312–3329

Aharoni C, Tompkins FC (1970) Kinetics of adsorption and desorption and the Elovich equation. Adv Catal 21(C):1–49

Ahmed MJ, Dhedan SK (2012) Equilibrium isotherms and kinetics modeling of methylene blue adsorption on agricultural wastes-based activated carbons. Fluid Phase Equilib 317:9–14

Amiri M, Shahhosseini S, Ghaemi A (2017) Optimization of CO_2 capture process from simulated flue gas by dry regenerable alkali metal carbonate based adsorbent using response surface methodology. Energy Fuels 31(5):5286–5296

Bahadori A, Vuthaluru HB (2009) New method accurately predicts carbon dioxide equilibrium adsorption isotherms. Int J Greenh Gas Control 3(6):768–772

Brockner W, Ehrhardt C, Gjikaj M (2007) Thermal decomposition of nickel nitrate hexahydrate, Ni $(NO_3)_2{\cdot}6H_2O$, in comparison to Co $(NO_3)_2{\cdot}6H_2O$ and Ca $(NO_3)_2$ $4H_2O$. Thermochim Acta 456(1):64–68

Carabineiro SA, McKee DW, Silva IF (2001) Uncatalysed and catalysed CO_2 reaction using metal catalysts and binary vanadium mixtures supported on activated carbon. Carbon 39(3):451–463

Das B et al (2013) Removal of copper from aqueous solution using alluvial soil of Indian origin: equilibrium, kinetic and thermodynamic study. J Mater Environ Sci 4(4):392–408

Deraz NM (2018) The comparative jurisprudence of catalysts preparation methods: I. Precipitation and impregnation methods. J Ind Environ Chem 2(1):19–21

Fashi F, Ghaemi A, Moradi P (2019) Piperazine-modified activated alumina as a novel promising candidate for CO2 capture: experimental and modeling. Greenh Gases Sci Technol 9(1):37–51

Fenrong Li et al (2010) Adsorption of carbon dioxide by coconut activated carbon modified with Cu/Ce. J Rare Earths 28:334–337

Freundlich H (1907) Über die adsorption in lösungen. Z Phys Chem 57(1):385–470

Gardner TJ, Messing GL (1984) Magnesium salt decomposition and morphological development during evaporative decomposition of solutions. Thermochim Acta 78(1–3):17–27

Ghaedi AM et al (2019) Optimization and modeling of simultaneous ultrasound-assisted adsorption of ternary dyes using copper oxide nanoparticles immobilized on activated carbon using response surface methodology and artificial neural network. Ultrason Sonochem 51:264–280

Hakim A et al (2015) Study of CO_2 adsorption and desorption on activated carbon supported iron oxide by temperature programmed desorption. Jurnal Teknologi 77(33):75–84

Hameed BH, Salman JM, Ahmad AL (2009) Adsorption isotherm and kinetic modeling of 2, 4-D pesticide on activated carbon derived from date stones. J Hazard Mater 163(1):121–126

Henning K-D, Schäfer S (1993) Impregnated activated carbon for environmental protection. Gas Sep Purif 7(4):235–240

Herawan SG et al (2013) Characterization of activated carbons from oil-palm shell by CO2 activation with no holding carbonization temperature. Sci World J. https://doi.org/10.1155/2013/624865

Heydarifard M et al (2018) Reactive absorption of CO_2 into piperazine aqueous solution in a stirrer bubble column: modeling and experimental. Int J Greenhouse Gas Control 79:91–116

Hidayu AR, Muda N (2016) Preparation and characterization of impregnated activated carbon from palm kernel shell and coconut shell for CO_2 capture. Procedia Eng 148:106–113

Ho Y-S, McKay G (1999) Pseudo-second order model for sorption processes. Process Biochem 34(5):451–465

Hosseini S et al (2015) Adsorption of carbon dioxide using activated carbon impregnated with Cu promoted by zinc. J Taiwan Inst Chem Eng 52:109–117

Houshmand A, Daud WMAW, Shafeeyan MS (2011) Exploring potential methods for anchoring amine groups on the surface of activated carbon for CO_2 adsorption. Sep Sci Technol 46(7):1098–1112

Jang D-I, Park S-J (2012a) Influence of nickel oxide on carbon dioxide adsorption behaviors of activated carbons. Fuel 102:439–444

Khajeh Amiri M, Ghaemi A, Arjomandi H (2019) Experimental, kinetics and isotherm modeling of carbon dioxide adsorption with 13X zeolite in a fixed bed column. Iranian J Chem Eng (IJChE) 16(1):54–64

Khajeh M, Ahad G (2019) Nanoclay montmorillonite as an adsorbent for CO_2 capture: experimental and modeling. J Chinese Chem Soc. https://doi.org/10.1002/jccs.201900150

Kim B-J, Cho K-S, Park S-J (2010) Copper oxide-decorated porous carbons for carbon dioxide adsorption behaviors. J Colloid Interface Sci 342(2):575–578

Lagregren S (1898) About the theory of so-called adsorption of soluble substances. Kungl Sven Veten Akad Handl 24:1–39

Langmuir I (1916) The constitution and fundamental properties of solids and liquids. Part L. Solids. J Am Chem Soc 38(11):2221–2295

Madura JD , Herring FG, Petrucci RH, Bissonnette C (1972) General chemistry: principles and modern applications

Madzaki H et al (2018) Carbon dioxide adsorption on activated carbon hydrothermally treated and impregnated with metal oxides. J Kejuruter 30(1):31–38

Míguez JL et al (2018) Evolution of CO_2 capture technology between 2007 and 2017 through the study of patent activity. Appl Energy 211:1282–1296

Mikuli E et al (2001) Melting and thermal decomposition of [Ni$(H_2O)_6$]$(NO_3)_2$. Thermochim Acta 370(1–2):65–71

Mohammad NK, Ghaemi A, Tahvildari K (2019) Hydroxide modified activated alumina as an adsorbent for CO_2 adsorption: experimental and modeling. Int J Greenhouse Gas Control 88:24–37

Karbalaei Mohammad N et al (2019) Experimental investigation and modeling of CO_2 adsorption using modified activated carbon. Iran J Chem Chem Eng (IJCCE) 39(1):177–192

Norouzbahari S, Shahhosseini S, Ghaemi A (2016) Chemical absorption of CO_2 into an aqueous piperazine (PZ) solution: development and validation of a rigorous dynamic rate-based model. RSC Adv 6(46):40017–40032

Pashaei H et al (2020) Experimental Modeling and Optimization of CO_2 Absorption into Piperazine Solutions Using RSM-CCD Methodology. ACS Omega. https://doi.org/10.1021/acsomega.9b03363

Pietrzak R, Morawski AW (2013) MgO/CaO-loaded activated carbon for carbon dioxide capture: practical aspects of use. Ind Eng Chem Res

Plaza MG et al (2010) Ammoxidation of carbon materials for CO_2 capture. Appl Surf Sci 256(22):6843–6849

Rashidi NA, Yusup S (2016) An overview of activated carbons utilization for the post-combustion carbon dioxide capture. J CO2 Util 13:1–16

Saeidi M et al (2018) Exploiting response surface methodology (RSM) as a novel approach for the optimization of carbon dioxide adsorption by dry sodium hydroxide. J Chin Chem Soc 65(12):1465–1475

Saeidi M, Ghaemi A, Tahvildari K (2019) CO2 capture exploration on potassium hydroxide employing response surface methodology, isotherm and kinetic models. Iran J Chem Chem Eng (IJCCE) 39(5):255–267

Sarrai AE et al (2016) Using central composite experimental design to optimize the degradation of tylosin from aqueous solution by photo-fenton reaction. Materials 9(6):428

Schwickardi M et al (2002) High-surface-area oxides obtained by an activated carbon route. Chem Mater 14(9):3913–3919

Shafeeyan MS et al (2011) Ammonia modification of activated carbon to enhance carbon dioxide adsorption: effect of pre-oxidation. Appl Surf Sci 257(9):3936–3942

Shafeeyan MS et al (2012) The application of response surface methodology to optimize the amination of activated carbon for the preparation of carbon dioxide adsorbents. Fuel 94:465–472

Shekhawat D, Luebke DR, and Pennline HW (2003) A review of carbon dioxide selective membranes: a topical report. National Energy Technology Laboratory (NETL), Pittsburgh, PA, Morgantown, WV

Sips R (1948) On the structure of a catalyst surface. J Chem Phys 16(5):490–495

Siriwardane RV et al (2001) Adsorption of CO_2 on molecular sieves and activated carbon. Energy Fuels 15(2):279–284

Somy A et al (2009) Adsorption of carbon dioxide using impregnated activated carbon promoted by Zinc. Int J Greenhouse Gas Control 3(3):249–254

Son S-J et al (2005) Development of carbon dioxide adsorbents using carbon materials prepared from coconut shell. Korean J Chem Eng 22(2):291–297

Taheri FS et al (2019) High CO_2 adsorption on amine-functionalized improved mesoporous silica nanotube as an eco-friendly nanocomposite. Energy Fuels 33(6):5384–5397

Thommes M et al (2015) Physisorption of gases, with special reference to the evaluation of surface area and pore size distribution (IUPAC Technical Report). Pure Appl Chem 87(9–10):1051–1069

Tuinier MJ et al (2010) Cryogenic CO2 capture using dynamically operated packed beds. Chem Eng Sci 65(1):114–119

Versteeg GF, Van Swaaij WPM (1988) Solubility and diffusivity of acid gases (carbon dioxide, nitrous oxide) in aqueous alkanolamine solutions. J Chem Eng Data 33(1):29–34

Wang M et al (2011) Post-combustion CO_2 capture with chemical absorption: a state-of-the-art review. Chem Eng Res Des 89(9):1609–1624

Yi H et al (2014) Simultaneous removal of SO 2, NO, and CO_2 on metal-modified coconut shell activated carbon. Water Air Soil Pollut 225(5):1965

Yong Z, Mata VG, Rodrigues AE (2001) Adsorption of carbon dioxide on chemically modified high surface area carbon-based adsorbents at high temperature. Adsorption 7(1):41–50

Younas M et al (2016) Feasibility of CO 2 adsorption by solid adsorbents: a review on low-temperature systems. Int J Environ Sci Technol 13(7):1839–1860

Zhou K, Li L, Ma X, Mo Y, Chen R, Li H, Li H (2018) Activated carbons modified by magnesium oxide as highly efficient sorbents for acetone. RSC Adv 8(6):2922–2932

Zieliński M et al (2005) Hydrogen storage on nickel catalysts supported on amorphous activated carbon. Catal Commun 6(12):777–783